Supporting Information

Novel microstructure-controlled Li ion conductive oxide-based ceramic solid electrolytes supporting high current densities

Nataly Carolina Rosero-Navarro[a*], Haruna Watanabe[b], Randy Jalem[c,d], Shota Sugio[b], Hiroaki Ito[b], Yoshitaka Tateyama[c,d], Akira Miura[a] and Kiyoharu Tadanaga[a]

[a.] Division of Applied Chemistry, Faculty of Engineering, Hokkaido University, Sapporo 060-8628, Japan

[b.] Graduate School of Chemical Sciences and Engineering, Hokkaido University, Sapporo 060-8628, Japan

[c.] Center for Green Research on Energy and Environmental Materials & Global Research Center for Environment and Energy based on Nanomaterials Science (GREEN), National Institute for Materials Science (NIMS), Tsukuba, Japan

[d.] Elements Strategy Initiative for Catalysts & Batteries, Kyoto University, Kyoto, Japan

*E-mail address: rosero@eng.hokudai.ac.jp

TABLE OF CONTENTS

1. EXPERIMENTAL SECTION

1.1 Synthesis of LLZT and LLZT-LBO solid electrolyte pellets

The solid electrolytes pellets were prepared following a reported procedure[1]. Precursors: $LiNO_3$ (99%, Kanto chemicals), $La(NO_3)_3{\cdot}6H_2O$ (99.9%, Kanto chemicals), $Ta(OC_2H_5)_5$ (99.9%, High-purity chemicals), $Zr(OC_4H_9)_4$ (85% in butanol, Wako pure chemicals) trimethoxyborane (TMB, Shin-Etsu Chemicals) and lithium ethoxide (High-purity chemicals). Ethyl acetoacetate (EAcAc, 99%, Kanto chemicals) and ethanol (super dehydrated, Wako) were used as complex agent and solvent, respectively.

For LLZT, $LiNO_3$ and $La(NO_3)_3{\cdot}6H_2O$ were dissolved in ethanol. $Ta(OC_2H_5)_5$, $Zr(OC_4H_9)_4$ and ethyl acetoacetate (EAcAc, 99%, Kanto chemicals) were dissolved in ethanol under argon atmosphere and stirred for 1 hour. Then, both solutions were mixed, and the resulted transparent solution was stirred at room temperature for 1 to 2 hours to obtain a sol. The obtained sol was dried under vacuum between 80 and 130 °C to obtain a dried gel that was later pulverized and heat-treated at 700 °C in an alumina crucible for 5 hours (1 °C min^{-1}). Finally, 2 g of this powder and 4 mL of toluene were placed in a ZrO_2 pot with ZrO_2 balls (Ø = 2 mm) and grounded at 300 RPM for 6 hours. Then, toluene was evaporated under vacuum at 100 °C to obtain final LLZT calcined powder. The molar ratio of Li:La:Zr:Ta:EAcAc was 7.15:3:1.4:0.5:1.45 and lithium was added in 10% excess to compensate for the loss of Li during sintering.

For LBO, TMB was dissolved in ethanol and stabilized by addition of EAcAc under argon atmosphere. Then, 0.1 M HNO_3 was added dropwise (molar ratio TMB:HNO_3 of 1:0.5), and

the mixture was stirred for 1 hour. In parallel, lithium ethoxide was dissolved in ethanol. Then, both solutions, TMB and lithium ethoxide, were mixed and stirred for 1 hour to obtain a precursor LBO solution. Molar ratio of TMB and lithium ethoxide (High-purity chemicals) was 3:1 and total concentration of 40 gL^{-1}.LBO (0.5 wt%) was added to the LLZT calcined powder and mixed in a mortar using toluene. Toluene was completely removed at 80 °C for approximately 2 hours.

The LLZT and LLZT-LBO calcination powders were formed into pellets (Ø = 10 mm) at 100 MPa (5 min) using a uniaxial press and then, were sintered at 1000 ºC (10 h) using a heating rate of 1 ºC/min and intermedium step at 700 ºC (5 h). The pellets were sintered under ambient atmosphere using alumina crucibles. The pellets were thoroughly buried in identical powder to mitigate losses of lithium and prevent any contamination with crucibles. The relative density of LLZT and LLZT-LBO pellets was 90+/-1% and 88+/-1% (theoretical density 5.11 g cm^{-3}), respectively.

1.2 Characterization

Crystal phase was determined by X-ray diffraction (XRD) using a RINT 2000 Ultima RIGAKU diffractometer. Powder samples were scanned between 10º and 60º at a rate of 2°/min using Cu-Kα radiation. Synchrotron X-ray diffraction patterns were measured at the BL02B2 beam line of Spring-8 (Proposal No. 2021A1573). The wavelength of the incident X-rays was 0.495810(1) Å. Morphology of the surface and cross-section solid electrolytes

were observed by scanning electron microscopy (SEM), performed on a JIB-4600F Multibeam SEM-FIB Scanning Electron Microscope.

The Vienna ab initio simulation package (VASP), which implements the generalized gradient approximation (GGA) approach and employs the projector-augmented wave (PAW) basis set, was used for density functional theory (DFT) calculations in this work.[2-3] For the Li_3BO_3, the reported stable phase with a $P2_1/c$ space group was adopted and its crystal structure information was taken from the Inorganic Crystal Structure Database (ICSD).[4] The structure of crystalline Li_3BO_3 (LBO) was used as a representative for the amorphous LBO, noting that in the short-range order, both are formed by similar BO_3^{-3} structural units.[5]

For comparison, the garnet solid electrolyte $Li_7La_3Zr_2O_{12}$ with the reported stable phase in the $I4_1/acd$ symmetry was also calculated. The geometry optimization step used the following settings: a kinetic energy cutoff of 520 eV, spin-polarized calculation, and at least a 1000 k-point Monkhorst–Pack mesh.[6] Standard pseudopotentials were chosen for Si, O, and La, while the potentials with the s shell treated as valence states were selected for Li and Zr. Convergence was ensured to satisfy <1 meV/atom and <0.01 eV $Å^{-1}$ in energy and residual forces, respectively. To evaluate the (electro)chemical reaction in the reductive and oxidative voltage regime or when Li_3BO_3 (or $Li_7La_3Zr_2O_{12}$) is in contact with the Li metal anode (i.e., high Li chemical potential condition) or with the cathode (i.e., low Li chemical potential condition), the Li grand potential phase diagram was constructed using known competing phases extracted from the Materials Project.[7-9] Additional phases not included in the latter

were taken from ICSD and were separately calculated by DFT to determine their total energies.

For analysis of Li-ion transport into the lithium borate, the climbing-image nudged elastic band (cNEB) method was carried out using a 3 × 1 × 1 supercell (84 atoms).[10] Numerical integration over the Brillouin zone was done by sampling the Γ-point. Convergence was confirmed to less than 10 meV/f.u in energy.

1.3 Symmetric cells for electrochemical characterization

The electrochemical properties of the pellets were investigated using gold blocking and lithium nonblocking electrodes. The measurement was conducted under an argon atmosphere. Gold blocking electrodes (circular electrodes of a diameter of 0.6 cm) were prepared by sputter-coating onto both sides of the pellet. Lithium metal (thickness 0.25 mm, diameter 6 mm) was attached to both sides of Au-coated solid electrolytes pellets in a glove box in a dry argon atmosphere, and a symmetric cell was assembled using a HS Flat cell HS-3ETK (Hohsen Corporation). The cell was heat treated at 175 ° C for 3 hours to promote the adhesion of the lithium to the garnet solid electrolyte[11].

Impedance spectra were recorded between ca. 0.01 Hz and 10 MHz using an impedance analyzer (Solartron SI1260) at the amplitude of 50-100 mV. Galvanostatic cyclic measurements of symmetric cells constructed with the garnet solid electrolyte modified with gold coating and lithium metal were carried out under variable current densities starting from a constant current density of 0.1 to 10 mA cm^{-2}. Each galvanostatic step was carried out

during 60. Long-term constant current measurements for lithium dissolution and precipitation reactions were performed at 0.1 mA cm^{-2} and 10 mA cm^{-2}.

2. SUPPORTING FIGURES

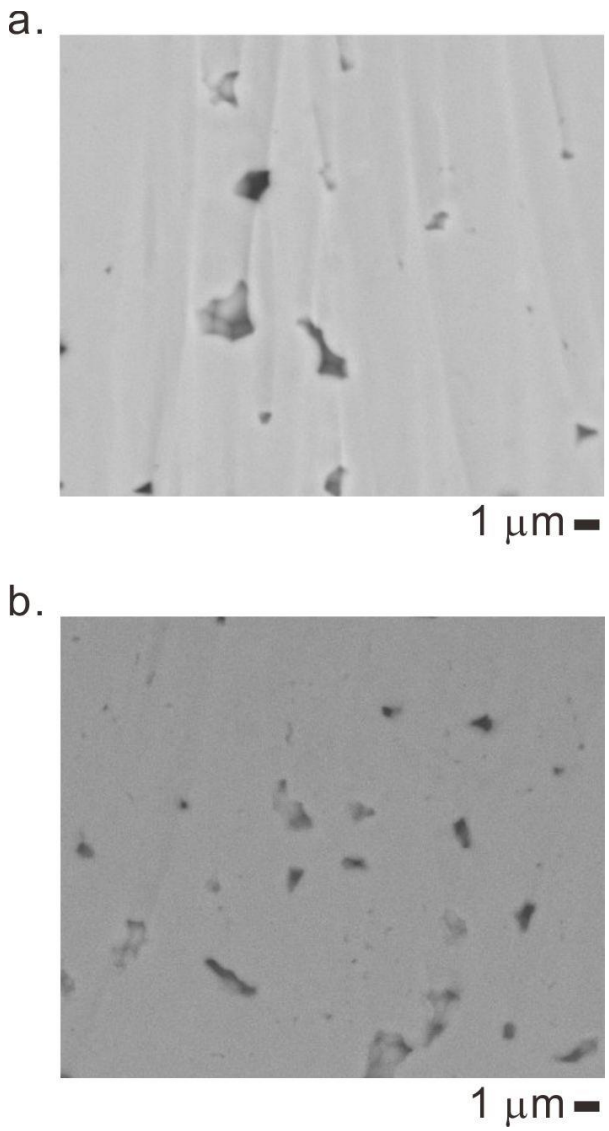

Figure S1. Polished cross-section SEM images of b) LLZT and c) LLZT-LBO.

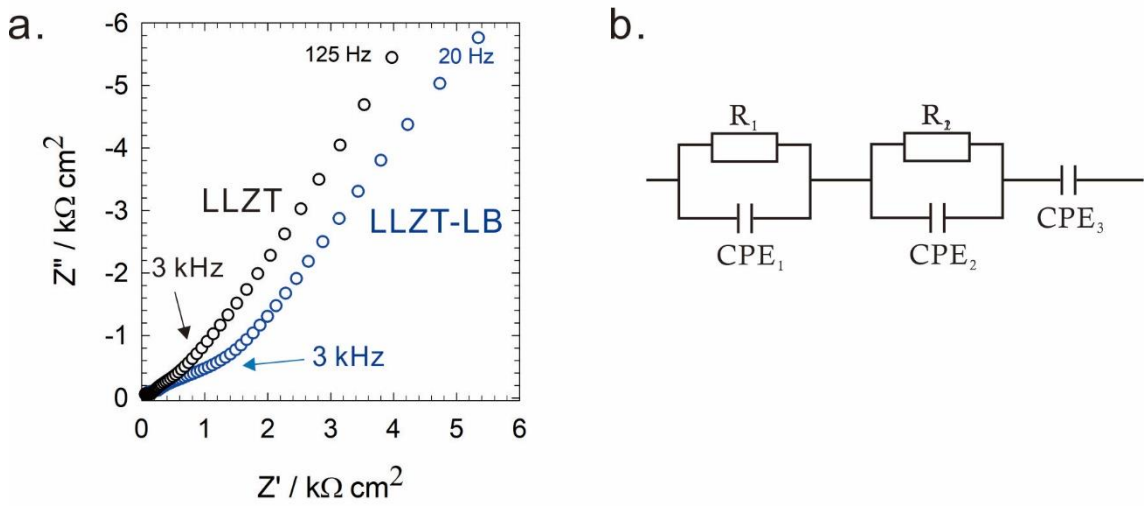

Figure S2. a) Nyquist plot of LLZT and LLZT-LBO at 25 °C. Equivalent Circuits used to fit the impedance profile of LLZT and LLZT-LBO in Figure 2d-g.

This should be noted that limited information at high frequencies can induce uncertainty in the assigned values for the contributions of grain and grain boundary resistances. To reduce the error, the equivalent circuits used to fit the impedance profiles are the simplest solution possible with two R||CPE associated with grain and grain boundary resistances. The goodness of fit remains in the order of 10^{-5}. R represents the resistance and CPE the constant phase element, which is characterized by two parameters C and n. The capacitance can be calculated from $CPE = (R^{1-n}C)^{1/n}$.

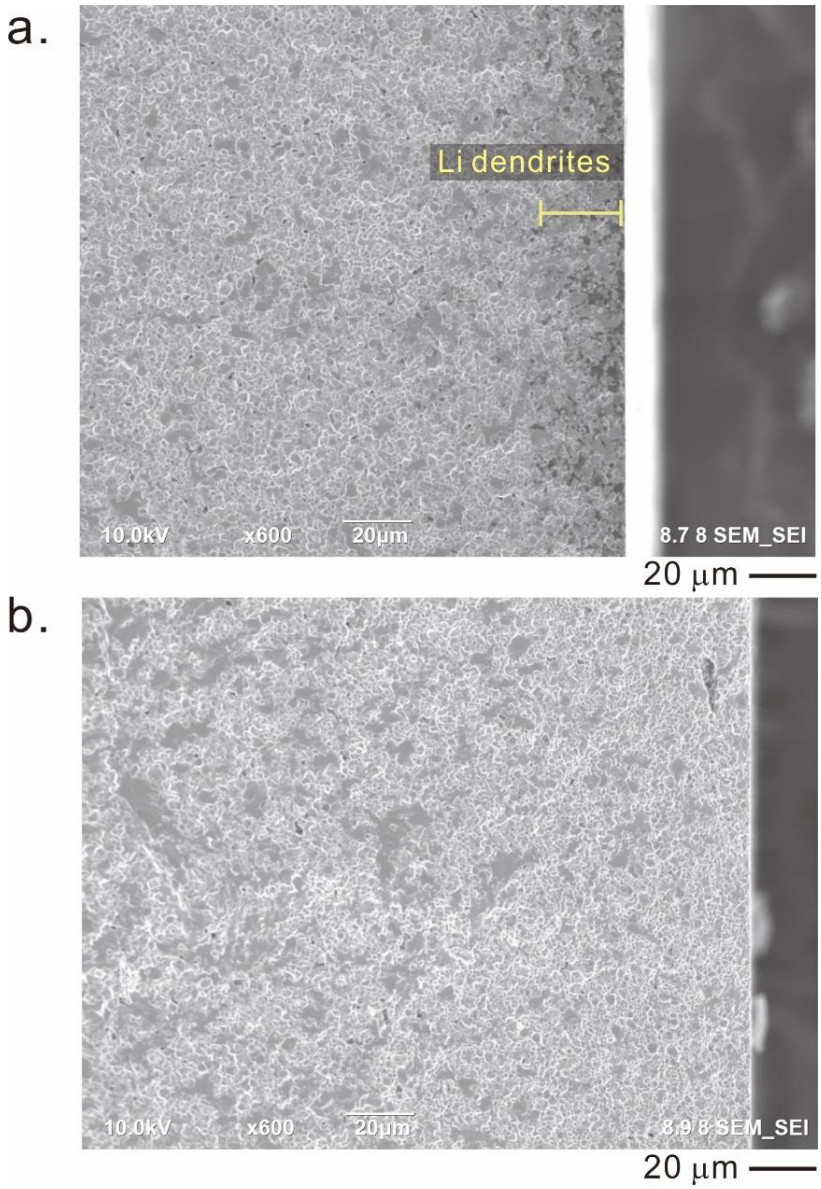

Figure S3. Low magnification cross-sectional SEM images of the LLZT and LLZT-LBO pellets after DC cycling measurement.

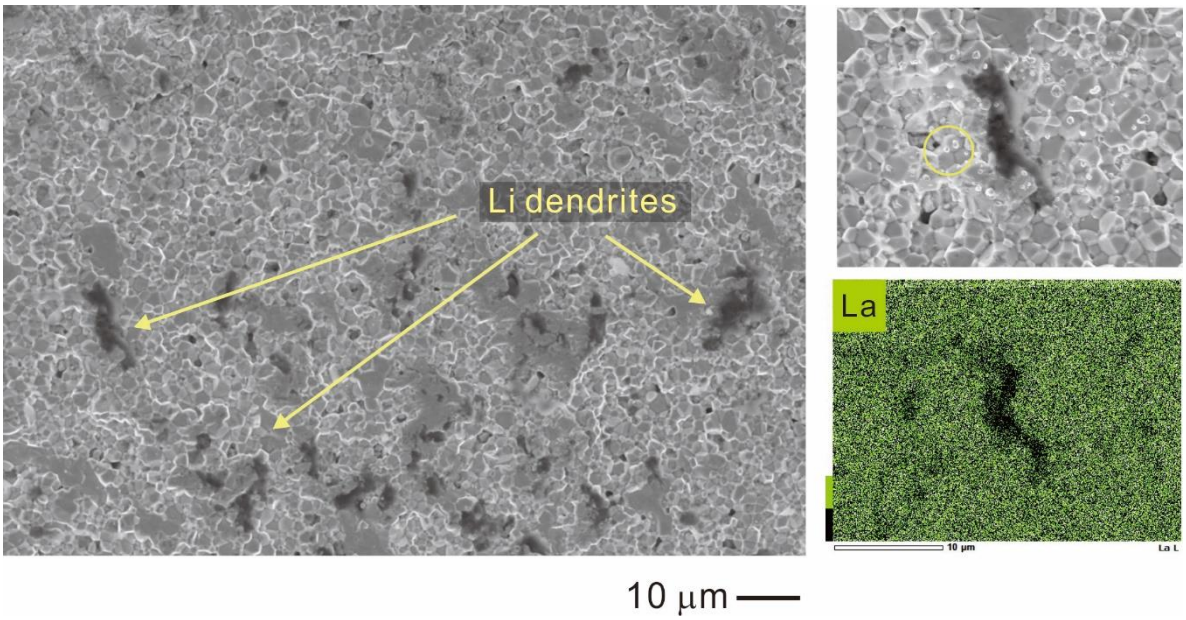

Figure S4. Low magnification surface SEM images of the LLZT pellet after DC cycling measurement. Energy-dispersive spectroscopy (EDS) analysis including lanthanum.

The LLZT surface was gently removed with a diamond pin to obtain the image of dendrites into the pellet. The yellow circle is highlighting the high reactivity of the surface during EDS analysis and is associated with de lithium reactivity close to the formed lithium dendrites.

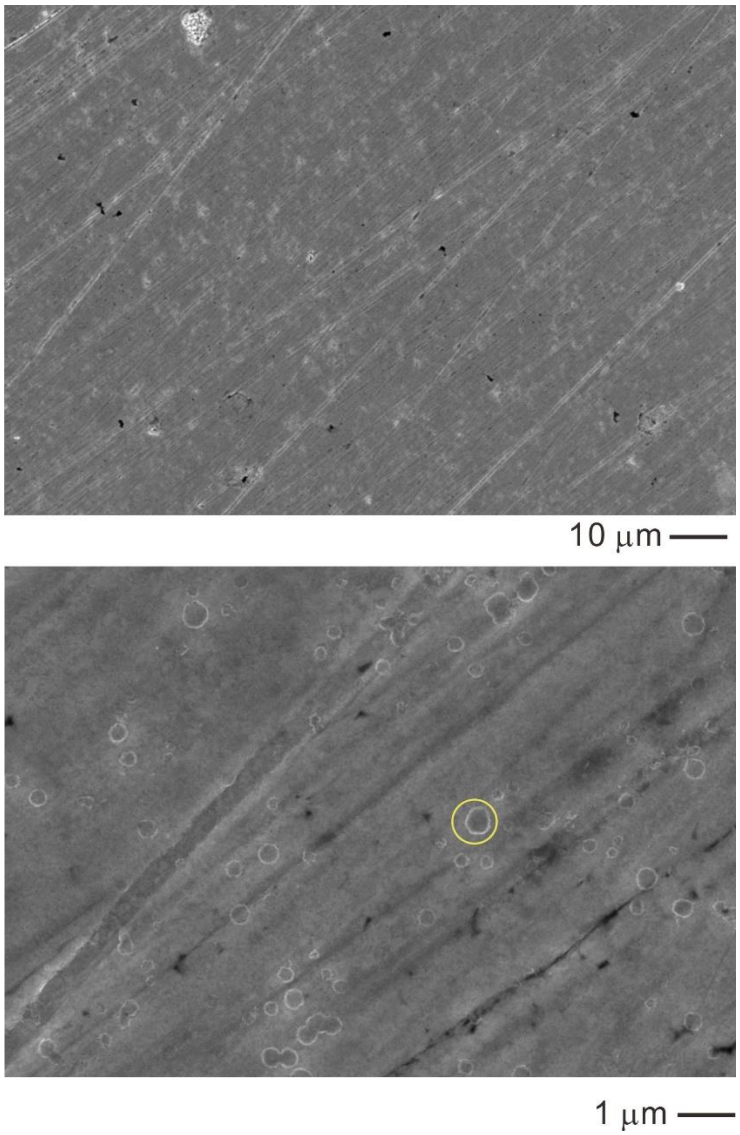

Figure S5. Low magnification surface SEM images of the LLZT-LBO pellet after DC cycling measurement.

The LLZT-LBO surface shows a smooth surface free of lithium dendrites is observed. The polishing tracks can be also easily observed. The yellow circle (bottom) is highlighting the high reactivity of the surface during SEM analysis and is associated with de lithium nucleation with the beam of the microscopy.

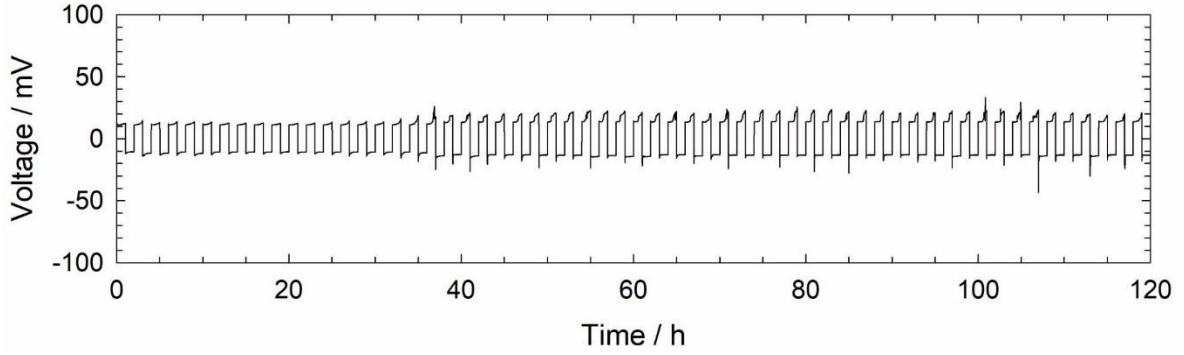

Figure S6. Direct current (DC) cycling measurement of the a) Li/LLZT/Li and b) Li/LLZT-LBO/Li cells at 10 mA cm^{-2} and 25 °C.

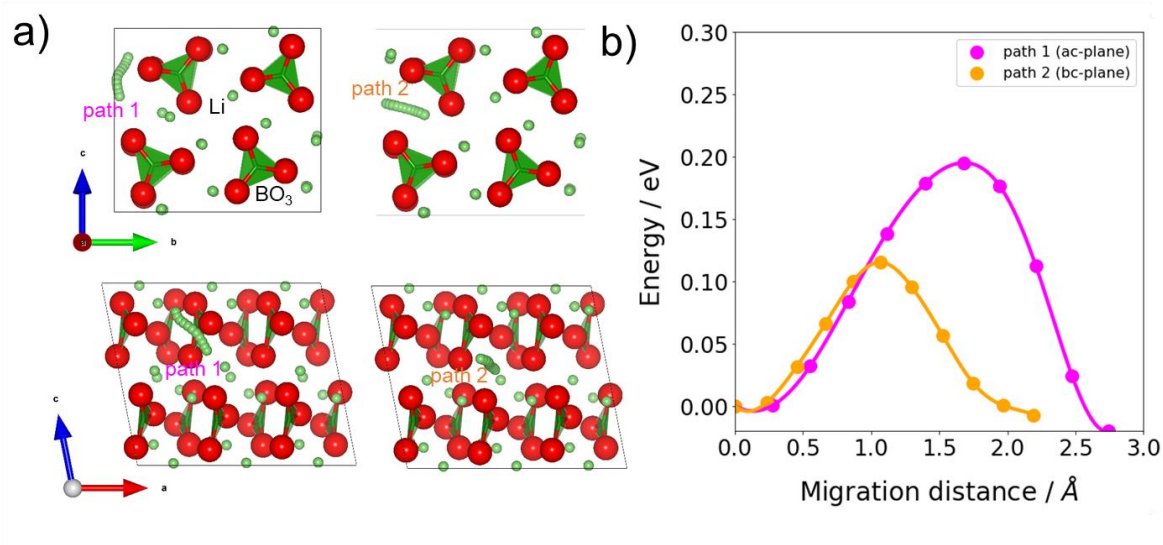

Figure S7. a) Li^+ ion migration trajectory (vacancy mechanism) and their corresponding b) energy profiles as calculated by DFT climbing-image nudged elastic band method.

References

1. Rosero-Navarro, N. C.; Watanabe, H.; Miura, A.; Tadanaga, K., Synthesis of highly Li-ion conductive garnet-type solid ceramic electrolytes by solution-process-derived sintering additives. *Journal of the European Ceramic Society* **2021**.

2. Kresse, G.; Hafner, J., Ab initio molecular dynamics for liquid metals. *Phys. Rev. B* **1993,** *47*, 558.

3. Perdew, J. P.; Wang, Y., Accurate and simple analytic representation of the electron-gas correlation energy. *Phys. Rev. B* **1992,** *45*, 13244.

4. Allen, F. H.; Bergerhoff, G.; Sievers, R., *Crystallographic Databases*. 1987.

5. Lelong, G.; Cormier, L.; Hennet, L.; Michel, F.; Rueff, J.-P.; Ablett, J. M.; Monaco, G., Lithium borate crystals and glasses: How similar are they? A non-resonant inelastic X-ray scattering study around the B and O K-edges. *Journal of Non-Crystalline Solids* **2017,** *472*, 1-8.

6. Monkhorst, H. J.; Pack, J. D., Special points for Brillouin-zone integrations. *Physical Review B* **1976,** *13* (12), 5188-5192.

7. Jain, A.; Ong, S. P.; Hautier, G.; Chen, W.; Richards, W. D.; Dacek, S.; Cholia, S.; Gunter, D.; Skinner, D.; Ceder, G.; Persson, K. A., Commentary: The Materials Project: A materials genome approach to accelerating materials innovation. *APL Mater.* **2013,** *1* (1), 11.

8. Ong, S. P.; Richards, W. D.; Jain, A.; Hautier, G.; Kocher, M.; Cholia, S.; Gunter, D.; Chevrier, V. L.; Persson, K. A.; Ceder, G., Python Materials Genomics (pymatgen): A robust, open-source python library for materials analysis. *Comput. Mater. Sci.* **2013,** *68*, 314-319.

9. Zhu, Y. Z.; He, X. F.; Mo, Y. F., Origin of Outstanding Stability in the Lithium Solid Electrolyte Materials: Insights from Thermodynamic Analyses Based on First-Principles Calculations. *ACS Appl. Mater. Interfaces* **2015,** *7* (42), 23685-23693.

10. Henkelman, G.; Uberuaga, B. P.; Jonsson, H., A climbing image nudged elastic band method for finding saddle points and minimum energy paths. *J. Chem. Phys.* **2000,** *113* (22), 9901-9904.

11. Inada, R.; Yasuda, S.; Hosokawa, H.; Saito, M.; Tojo, T.; Sakurai, Y., Formation and Stability of Interface between Garnet-Type Ta-doped $Li_7La_3Zr_2O_{12}$ Solid Electrolyte and Lithium Metal Electrode. *Batteries* **2018,** *4* (2), 26.